

# FLASC: A Flare-Sensitive Clustering Algorithm

Daniël M. Bot<sup>1</sup>, Jannes Peeters<sup>1</sup>, Jori Liesenborgs<sup>2</sup>, and Jan Aerts<sup>3</sup>

<sup>1</sup>Data Science Institute (DSI), UHasselt, Diepenbeek, Belgium

<sup>2</sup>Expertisecentrum voor Digitale Media (EDM), UHasselt – Flanders Make, Diepenbeek, Belgium

<sup>3</sup>Augmented Intelligence for Data Analytics (AIDA) Lab, Department of Biosystems, KU Leuven, Leuven, Belgium

## ABSTRACT

Clustering algorithms are often used to find subpopulations in exploratory data analysis workflows. Not only the clusters themselves, but also their shape can represent meaningful subpopulations. In this paper, we present FLASC, an algorithm that detects branches within clusters to identify such subpopulations. FLASC builds upon HDBSCAN\*—a state-of-the-art density-based clustering algorithm—and detects branches in a post-processing step that describes within-cluster connectivity. Two variants of the algorithm are presented, which trade computational cost for noise robustness. We show that both variants scale similarly to HDBSCAN\* in terms of computational cost and provide stable outputs using synthetic data sets, resulting in an efficient flare-sensitive clustering algorithm. In addition, we demonstrate the benefit of branch-detection on two real-world data sets.

Keywords: Exploratory data analysis, density-based clustering, branch-hierarchy detection, HDBSCAN\*

## INTRODUCTION

Exploratory Data Analysis (EDA)—i.e., searching for interesting patterns in data—is ubiquitous in data science and knowledge discovery workflows. Detecting which subpopulations exist in a data set is a common step in EDA. Typically, subpopulations are detected as clusters, which traditional algorithms model as Gaussian distributions (as cited in Campello et al. (2015)). More recently, density-based clustering has become more popular (e.g., Ester et al. (1996); Campello et al. (2013)). These algorithms, informally, specify clusters as regions of high density separated by regions of lower density, allowing them to capture cluster shapes, which may be non-convex and reveal relevant subpopulations. For example, a Y-shaped cluster might represent an evolving process with two distinct outcomes. Consequently, the branches in a cluster’s manifold—i.e., *flares*—can represent meaningful subpopulations (see also, Lum et al. (2013); Skaf and Laubenbacher (2022); Kamruzzaman et al. (2018); Reaven and Miller (1979)).

Clustering algorithms generally cannot detect this type of subgroup because there is no gap that separates flares from their cluster. From a topological perspective, clustering algorithms describe the connected components in a *simplicial complex* of the data (Carlsson, 2014): a set of points, edges, and triangles that describe connectivity. Flares are connected in the simplicial complex. In other words, there is a path between data points in different branches that exclusively goes through data points ‘that lie close together’. Therefore, they have a vanishing homology and cannot be detected as clusters.

Several flare-detection techniques have been proposed in topological data analysis literature. For example, Carlsson (2014) proposed *functional persistence* to distinguish flares from a data set’s central core. This technique quantifies data

point centrality as the sum of its distances. Central observations have lower distance sums than points towards the extreme ends of the feature space. A manually controlled centrality threshold then removes the data’s core, separating branches from each other and making them detectable as clusters.

Extending this approach to compute branching hierarchies requires considering both the centrality and the data point distances in what is called a *bi-filtration*. The centrality controls how much of the core is retained to describe how branches grow and merge. The data point distances determine whether points are connected and form a cluster. Algorithms for computing bi-filtrations are computationally expensive (Lesnick and Wright, 2022; Kerber and Rolle, 2021). Their resulting *bi-graded* hierarchies are also complicated to work with, as they do not have a compact representation (Carlsson, 2014) (though research into usable representations is ongoing (Botnan et al., 2022)), and existing visualisations are non-trivial (Lesnick and Wright, 2015; Scoccola and Rolle, 2023). Alternative strategies that simultaneously vary both dimensions in a single-parameter filtration exist (Chazal et al., 2009); however, they remain computationally expensive (Vandaele et al., 2021).

In the present paper, we present an approach that efficiently computes branching hierarchies and detects branch-based subgroups of clusters in unfamiliar data. Inspired by Vandaele et al. (2021), we compute branching hierarchies using graph approximations of the data. This effectively replaces functional persistence’s manual centrality threshold with the question of which data points should be connected in the approximation graph. We will use HDBSCAN\* (Campello et al., 2013, 2015)—a state-of-the-art density-based clustering algorithm—to answer this question. Conceptually, our approach can be thought of as creating a sequence of subgraphs which progressively include more and more central points and tracking the remaining con-

nected components. Interestingly, a similar method has been used by Li et al. (2017) to detect *actual* branches in 3D models of plants.

Our main contribution is this flare detection approach, implemented as a post-processing step in McInnes et al. (2017)’s HDBSCAN\* implementation<sup>1</sup> and as a stand-alone package<sup>2</sup>. We propose two types of approximation graphs that naturally arise from HDBSCAN\*’s design and provide a practical centrality metric for points within a cluster that is computable with a linear complexity. Combining density-based clustering and flare detection into a single algorithm provides several attractive properties:

- The ability to detect clusters and their branches.
- No manual thresholds, instead intuitive minimum cluster and branch sizes control the detected subgroups.
- Low computational cost compared to multi-parameter persistence and other structure learning algorithms.
- High branch-detection sensitivity and noise robustness by operating on HDBSCAN\*-clusters, which suppress spurious noisy connectivity.
- Branch-detection at multiple distance scales because each cluster has its own approximation graph.

We call the resulting algorithm flare-sensitive clustering (FLASC) and empirically analyse its computational cost and stability on synthetic data sets to show that the flare detection cost is relatively low. In addition, we demonstrate FLASC on two real-world data sets, illustrating its benefits for data exploration.

The remainder of this article is organised as follows: Section ‘Related Work’ provides a literature overview of related data analysis algorithms and describes the HDBSCAN\* algorithm in more detail. Section ‘The FLASC Algorithm’ describes how FLASC builds on HDBSCAN\* to detect branches within clusters and discusses the algorithm’s complexity and stability. Section ‘Experiments’ presents our empirical analyses that demonstrate the algorithm’s computational complexity, stability, and benefits for data exploration. Finally, Sections ‘Discussion’ and ‘Conclusion’ discuss our results and present our conclusions.

## RELATED WORK

The purpose of our work is detecting branching structures within clusters. As such, our work relates to manifold and structure learning algorithms in general. In this section, we provide an overview of related data analysis algorithms and introduce HDBSCAN\*, the density-based clustering algorithm we build upon.

### Structure Learning

Many types of data lie not just on a manifold, but on a smooth, one-dimensional structure. Extracting these structures can be essential in unsupervised learning applications. For example, road

networks can be extracted from GPS measurements (Bonnaire et al., 2022) and cell developmental trajectories can be extracted from gene expression data (Qiu et al., 2017; Vandaele et al., 2020). Algorithms for extracting such structures are related to our work because the branch-based subgroups we are interested in can be extracted from them by partitioning the data between their intersections (Chervov et al., 2020).

Most work on extracting smooth, one-dimensional manifolds is based on Hastie and Stuetzle (1989)’s concept of *principal curves*: a smooth, self-consistent curve that passes through the middle of the data. Techniques estimating principal curves, trees, or graphs are often based on Expectation Maximisation (Dempster et al., 1977) and optimise the one-dimensional manifold directly (e.g., Bonnaire et al. (2022); Mao et al. (2017)). Alternative approaches are more closely related to non-linear Dimensionality Reduction (DR) algorithms that model the data’s structure as an undirected graph (e.g., Roweis and Saul (2000); Tenenbaum et al. (2000); Belkin and Niyogi (2003); van der Maaten and Hinton (2008); McInnes et al. (2020)). For example, Vandaele et al. (2020) use (manually) pruned minimum spanning trees over edges weighted by their boundary coefficient to extract a graph’s backbone. Alternatively, Ge et al. (2011) extract graph skeletons using a *Reeb Graph*. Reeb Graphs track the existence, merges, and splits of connected components in level sets of a continuous function defined on a manifold. Using geodesic distances to an arbitrary eccentric point as the continuous function makes the Reeb Graph capture the manifold’s skeleton. Interestingly, Mapper—an algorithm that approximates Reeb Graphs (Singh et al., 2007)—has also been used for detecting branch-based subpopulations (Kamruzzaman et al., 2018).

There are several similarities between these methods and our work. Like Vandaele et al. (2020), our approach detects tree-based branching hierarchies. Like Ge et al. (2011), our approach is topologically inspired. Where they create a Reeb Graph, we compute a Join Tree. The main difference of these methods compared to our work is their goal. We aim to identify relevant branch-based subpopulations. Ge et al. (2011), Vandaele et al. (2020), and the expectation maximisation-based algorithms explicitly model the data’s structure which necessitates a larger computational cost.

### HDBSCAN\*

HDBSCAN\* is a density-based clustering algorithm that provides state-of-the-art clustering performance (Campello et al., 2013, 2015). Informally, density-based clustering specifies clusters as regions of high density separated by regions of lower density. This formulation does not limit clusters to convex shapes and provides a natural way to separate noise points from clusters. The algorithm is well suited for exploring unfamiliar data because—unlike older popular clustering algorithms—HDBSCAN\* does not require the number of clusters or the distance between clusters to be specified in advance.

Several studies have implemented and adapted the HDBSCAN\* algorithm: McInnes and Healy (2017) improved the algorithm’s computational performance by using *space trees*

<sup>1</sup>hdbscan: <https://github.com/scikit-learn-contrib/hdbscan>

<sup>2</sup>pyflasc: <https://github.com/vda-lab/pyflasc>

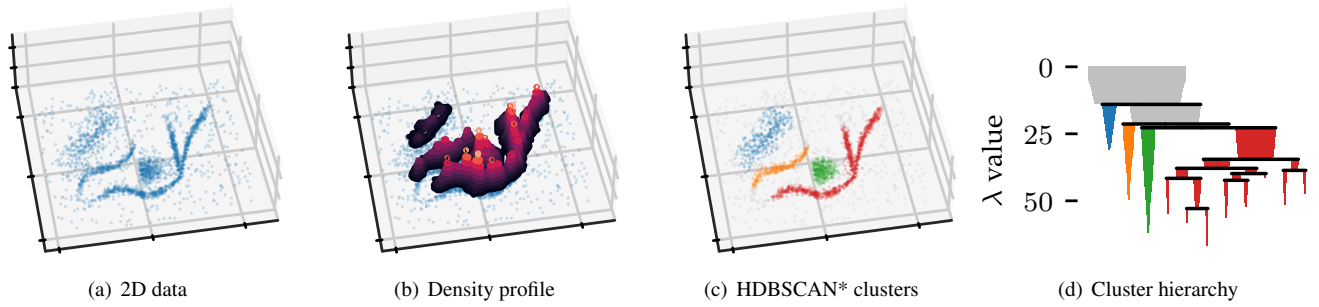


**Figure 1.** Density-based clustering concepts behind HDBSCAN\*. (a) A 2D example point cloud with varying density adapted from McInnes et al. (2022)’s online tutorial. (b) Density contours in a height map illustrate the data’s density profile. Peaks in this density profile correspond to *density contour clusters*. (c) Clusters extracted from the density profile by HDBSCAN\* indicated in colour. (d) The *density contour tree* describes how density contour clusters merge when considering lower density thresholds.

for finding the data points’ nearest neighbours and provide a popular and efficient Python implementation (McInnes et al., 2017). Stewart and Al-Khassaweneh (2022) created a Java implementation with a novel prediction technique for unseen data points. Jackson et al. (2018) presented an approximate HDBSCAN\* algorithm that uses NN-descent (Dong et al., 2011) for finding the nearest neighbours providing fast distributed performance. Malzer and Baum (2020) introduced a cluster selection distance threshold that effectively creates a hybrid between DBSCAN’s (Ester et al., 1996) and HDBSCAN\*’s cluster selection, improving the algorithm’s performance on data sets with small clusters and a large density variability. Neto et al. (2021) showed how Relative Neighbourhood Graphs (RNGs) (Tousaint, 1980) can be used to efficiently compute HDBSCAN\* cluster hierarchies for multiple *min cluster size* values. Their follow-up work presented MustaCHE, a visualisation tool for the resulting meta-cluster hierarchy (Neto et al., 2018). To our knowledge, no previous study has adapted HDBSCAN\* for detecting flares.

Because our work builds on HDBSCAN\*, it is relevant to explain how the algorithm works in more detail. The remainder of this section describes HDBSCAN\* following Campello et al. (2015)’s explanation. We refer the reader to McInnes and Healy (2017) for a more formal, statistically motivated description of the algorithm.

### The HDBSCAN\* Algorithm

HDBSCAN\* is based on density-based clustering concepts pioneered by Wishart (1969) and formalised by Hartigan (1975). We demonstrate these ideas using a 2D point cloud adapted from McInnes et al. (2022)’s online tutorial shown in Fig. 1(a). In general, let  $\mathbf{X} = \{\mathbf{x}_1, \dots, \mathbf{x}_N\}$  be a data set consisting of  $N$  feature vectors  $\mathbf{x}_{(i)}$  and a distance metric  $d(\mathbf{x}_i, \mathbf{x}_j)$ . Then, a point’s *core distance*  $\kappa(\mathbf{x}_i)$  is the distance to its  $k$ -nearest neighbour and HDBSCAN\* estimates its density as  $\lambda_k(\mathbf{x}_i) = 1/\kappa(\mathbf{x}_i)$  (Campello et al., 2015). Figure 1(b) illustrates the example’s density profile as contours in a height map. *Density contour clusters* intuitively correspond to peaks in the density profile, for example, the clusters indicated in colour in Fig. 1(c). More formally, the density contour clusters at some threshold  $\lambda_t$  are a collection of maximal, connected subsets in a level

set  $\{\mathbf{x} \mid \lambda(\mathbf{x}) \geq \lambda_t\}$  (Hartigan, 1975). In other words, density contour clusters are the connected components of points with a density larger than some threshold. *Density contour trees* capture the hierarchy in which density contour clusters merge as the density threshold decreases. From a topological perspective, density contour trees are a *join tree* of the data’s density profile.

Data sets generally do not have an inherent notion of connectivity between their data points. Such a notion is needed to determine whether two points are part of the same density contour cluster at a threshold  $\lambda_t$ . HDBSCAN\* solves this problem by considering points to be connected if the distance between them is smaller than or equal to  $1/\lambda_t$ . This solution is possible because density is defined in terms of distance. HDBSCAN\* uses a *mutual reachability* distance between points for this purpose, which is defined as (Campello et al., 2015):

$$d_{\text{reach}}(\mathbf{x}_i, \mathbf{x}_j) = \begin{cases} \max \{ \kappa(\mathbf{x}_i), \kappa(\mathbf{x}_j), d(\mathbf{x}_i, \mathbf{x}_j) \} & \text{if } \mathbf{x}_i \neq \mathbf{x}_j, \\ 0 & \text{otherwise,} \end{cases} \quad (1)$$

where the value of  $k$  as used in  $\kappa$  is specified manually and acts as a smoothing factor for the density estimation.

Using the mutual reachability distance to provide connectivity, we can now recover the density contour tree. The edges that change connectivity between density contour clusters are exactly those edges in the data’s Minimum Spanning Tree (MST) (see, f.i., Doraiswamy et al. (2021)). HDBSCAN\* uses a MST to efficiently compute a single linkage clustering hierarchy (Sibson, 1973). The resulting dendrogram is simplified using a manually specified minimum cluster size  $m_c$  to recover a condensed cluster hierarchy that resembles the data’s density profile as shown in Fig. 1(d). From the root down, only the sides of a split containing more than  $m_c$  points are considered to represent clusters. Sides with fewer points are interpreted as “falling out of the parent cluster” (McInnes and Healy, 2017) or the cluster disappearing completely.

HDBSCAN\* provides two strategies for selecting clusters from the condensed hierarchy: the *excess of mass* (EOM) strategy and the *leaf* strategy (Campello et al., 2015). The leaf strategy selects all leaf segments in the condensed hierarchy, typically resulting in multiple small clusters. The EOM strategy

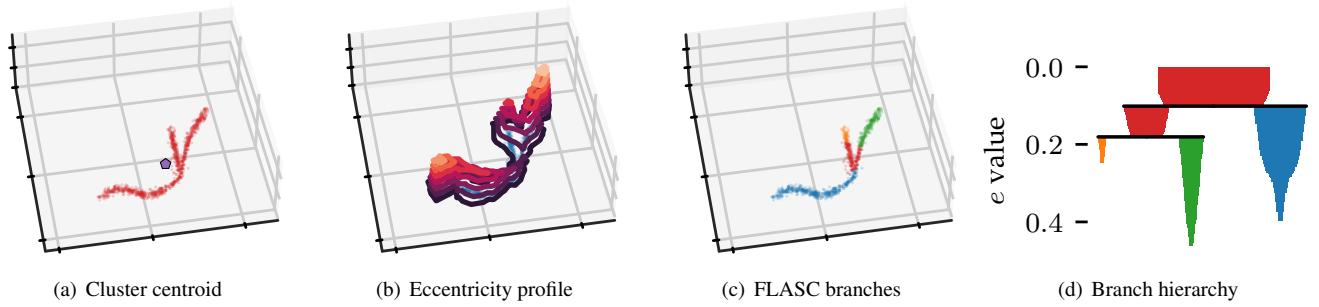


**Figure 2.** Density-based clustering concepts behind FLASC. (a) A within-cluster eccentricity  $e(\mathbf{x}_i)$  is defined for each point  $\mathbf{x}_i$  in cluster  $C_j$  based on distances to the cluster’s membership weighted average shown by the pentagon mark. (b) The cluster’s eccentricity profile visualised as contours on a height map. Peaks in the profile correspond to branches in the cluster. (c) Branches extracted from the cluster by FLASC indicated in colour. The cluster’s centre is given its own label. (d) The *eccentricity contour tree* describes how branches merge when considering lower eccentricity thresholds.

maximises relative cluster stability while preventing any data point from being a member of more than one selected cluster. A cluster  $C_j$ ’s relative stability  $\sigma_k(C_j)$  is defined as (Campello et al., 2015):

$$\sigma_k(C_j) = \sum_{\mathbf{x}_i \in C_j} \lambda_{k,\max}^{C_j}(\mathbf{x}_i) - \lambda_{k,\min}^{C_j}, \quad (2)$$

where  $\lambda_{k,\max}^{C_j}(\mathbf{x}_i)$  is the density at which  $\mathbf{x}_i$  falls out of  $C_j$  or  $C_j$  separates into two clusters, and  $\lambda_{k,\min}^{C_j}$  is the minimum density at which  $C_j$  exists. In words, the stability of a cluster is the sum of density ranges in which points are part of the cluster, which corresponds to the area of the cluster’s icicle in Fig. 1(d). HDBSCAN\*’s *cluster selection epsilon* parameter can be used to specify a minimum persistence for EOM clusters (Malzer and Baum, 2020).

## FLARE-SENSITIVE HDBSCAN\*

The main contribution of our work is a flare detection post-processing step for HDBSCAN\*. This section describes how the post-processing step works and integrates with HDBSCAN\* to form our FLASC algorithm (see Algorithm 1). FLASC starts by evaluating a flat HDBSCAN\* clustering, keeping track of the *space tree* used in HDBSCAN\* (McInnes et al., 2017; McInnes and Healy, 2017) to efficiently find nearest neighbours. One noteworthy change from McInnes et al. (2017)’s implementation is that we give all points the 0-label when a single cluster is allowed and selected and no *cluster selection epsilon* is applied. This enables FLASC to better analyse branching structures in data sets that contain a single cluster. Then, for each selected cluster  $C_j$ , a branch detection step is performed, explained in more detail below.

The concepts behind density-based clustering can also be applied to detect branches within clusters by using an eccentricity measure in place of density, as shown in Fig. 2. Peaks in an eccentricity profile correspond to branches in the cluster, as shown in Fig. 2(b) and Fig. 2(c). We define eccentricity as the distance to the cluster’s centroid:

$$e(\mathbf{x}_i) = d(\bar{\mathbf{x}}_{C_j}, \mathbf{x}_i), \quad (3)$$

where  $\bar{\mathbf{x}}_{C_j}$  is the cluster’s membership-weighted average (Fig. 2(a)). This eccentricity measure can be computed in  $\mathcal{O}(N)$ . Comparable to density contour clusters, an *eccentricity contour cluster* is a maximal, connected subset of points with an eccentricity larger than some threshold  $\{\mathbf{x} \mid e(\mathbf{x}) \geq e_t\}$ . As in functional persistence (Carlsson, 2014), eccentricity thresholds filter out cluster cores, which separates branches and makes them detectable as connected components.

Similar to HDBSCAN\*, we need a notion of connectivity between data points to determine whether two points are part of the same eccentricity contour cluster at a threshold  $e_t$ . In FLASC, we provide two solutions based on the cluster’s density scale in the form of *cluster approximation graphs*  $\mathbf{G}_k^{C_j}$ : the *full* approximation graph and the *core* approximation graph. Both types contain a vertex for each point in the cluster  $\mathbf{x}_i \in C_j$  but differ in which edges they include. The *full* approximation graph adds all edges with  $d_{mreach}(\mathbf{x}_i, \mathbf{x}_l) \leq d_{\max}^{C_j}$ , where  $d_{\max}^{C_j}$  is the largest distance in the cluster’s minimum spanning tree (MST). The resulting graph accurately describes the connectivity within the cluster at the density where the last point joins the cluster. The *space tree* constructed by HDBSCAN\* is used to retrieve these edges efficiently. The *core* approximation graph adds all edges with  $d_{mreach}(\mathbf{x}_i, \mathbf{x}_j) \leq \max\{\kappa(\mathbf{x}_i), \kappa(\mathbf{x}_j)\}$ . The resulting graph accurately describes the connectivity in the cluster’s MST. Alternatively, this graph can be considered as the cluster’s subgraph from the  $k$ -nearest neighbour graph over the entire data set. HDBSCAN\* already extracted these edges when the core distances were computed, so this approach has a lower additional cost.

We can now recover the eccentricity contour tree as if it is were density contour tree by applying HDBSCAN\*’s clustering steps to the cluster approximation graph with its edges weighted by  $\min\{e(\mathbf{x}_i), e(\mathbf{x}_l)\}$ . This weighting ensures an edge has the eccentricity of the least eccentric point it connects. Specifically, we adapt McInnes and Healy (2017)’s Union-Find data structure to construct a single linkage dendrogram. The resulting hierarchy is simplified using a minimum branch size  $m_b$  to recover the condensed branching hierarchy shown in Fig. 2(d).

HDBSCAN\*’s EOM and leaf strategies are used to com-

---

**Algorithm 1** A high-level overview of the FLASC algorithm.

---

```
1: function FLASC( $\mathbf{X}, d$ )
  ▷  $\mathbf{X}$  is a dataset with  $N$  feature vectors  $\mathbf{x}_{(\cdot)}$  and  $d$  is a distance metric  $d(\mathbf{x}_i, \mathbf{x}_j)$ .
2:   evaluate HDBSCAN( $\mathbf{X}, d$ ) and store its internal data structures.
3:   for each detected cluster  $C_j$  do
4:     compute the eccentricity  $e(\mathbf{x}_i)$  for all  $\mathbf{x}_i \in C_j$ .
5:     extract the cluster approximation graph  $\mathbf{G}_k^{C_j}$ .
6:     compute the single linkage clustering hierarchy of  $\mathbf{G}_k^{C_j}$ 
7:     simplify the clustering hierarchy using a minimum branch size  $m_b$ .
8:     extract labels and probabilities for a ‘flat’ clustering.
9:   end for
10:  combine the cluster and branch labels and probabilities.
11:  return the membership labels and probabilities.
12: end function
```

---

pute branch labels and membership probabilities from these condensed hierarchies. Points that enter the filtration after the selected branches have connected—i.e. points with the noise label—are given a single non-noise label representing the cluster’s centre. Finally, the cluster and branch labels are combined. By default, points in clusters with two or fewer branches are given a single label because two branches are expected in all clusters, indicating the outsides growing towards each other. The *label sides as branches* parameter can be used to turn off this behaviour and separate the ends of elongated clusters in the labelling. The cluster and branch probabilities are combined by taking their average value (Fig. 3(a)).

Other labelling and probability combinations are possible. For example, the cluster and branch probability product more strongly emphasises the outsides of the branches (Fig. 3(b)). As in McInnes et al. (2017), FLASC supports computing branch membership vectors that describe how strongly a point  $\mathbf{x}_i \in C_j$  belongs to each branch  $B_b \subset C_j$ . These membership values are based on the geodesic distances in the cluster approximation graph  $\mathbf{G}_k^{C_j}$ :  $d_{geo}(\mathbf{r}_{B_b}, \mathbf{x}_i)$ , where  $\mathbf{r}_{B_b}$  is the branch’s root, i.e., the point closest to the branch’s membership-weighted average  $\bar{\mathbf{x}}_{B_b}$ . The branch membership vectors can be used to label central points by the closest branch root, as in Fig. 3(c). Alternatively, a softmax function can be used to convert  $d_{geo}(\mathbf{r}_{B_b}, \mathbf{x}_i)$  into the membership probabilities:

$$p(\mathbf{x}_i, B_b) = \frac{e^{c_b(\mathbf{x}_i, B_b)/t}}{\sum_{B_l \in C_j} e^{c_b(\mathbf{x}_i, B_l)/t}}, \quad (4)$$

where  $c_b(\mathbf{x}_i, B_b) = 1/d_{geo}(\mathbf{r}_{B_b}, \mathbf{x}_i)$  and  $t$  is a temperature parameter (Fig. 3(d)).

Low persistent branches can be ignored using a *branch selection persistence* parameter, analogous to HDBSCAN\*’s *cluster selection epsilon* (Malzer and Baum, 2020). As branches do not necessarily start at zero centrality, *branch selection persistence* describes the minimum eccentricity range, rather than a single eccentricity threshold value. The procedure that applies the threshold simplifies the condensed branch hierarchy until all leaves have a persistence larger than the threshold.

### Stability

Stability is an important property of algorithms indicating that their output differs only slightly when the input changes slightly. Two notions of stability are relevant for FLASC: (1) the algorithm has to provide similar results when run repeatedly on (different) samples of an underlying distribution, and (2) the detected branch hierarchies have to represent the clusters’ underlying topology accurately. The deterministic density-based design of FLASC provides stability in the first sense.

Vandaele et al. (2021) analysed the second notion of stability for graph-based branch detection, explaining that the graph approximation should accurately represent the underlying shape and the graph-based centrality function should accurately describe the points’ centrality in a cluster’s metric space  $(C_j, d_{mreach})$ . For the *normalised centrality* used by Carlsson (2014), Vandaele et al. (2021) show that the bound on the bottleneck distances between true and empirical persistence diagrams is tight if the metric distortion induced by the graph and its maximum edge weight is small.

Both the *full* and *core cluster approximation graph* used by FLASC satisfy the low maximum edge weight requirement as their largest edge weight is the minimum mutual reachability distance required for all points in the cluster to be connected in the graph. Additionally, the metric distortion should be small as only edges in the local neighbourhood of data points are included because the clusters do not contain noise points.

The eccentricity function (Equation (3)) is more complex to analyse. It is a *c-Lipschitz-continuous* function when considered over the *cluster centrality graph*’s edges:

$$|\max\{e(\mathbf{x}_i), e(\mathbf{x}_j)\} - \max\{e(\mathbf{x}_k), e(\mathbf{x}_l)\}| \leq c \, d_{mreach}(\mathbf{x}_i, \mathbf{x}_l),$$

where  $c$  is a constant describing the continuity,  $(\mathbf{x}_i, \mathbf{x}_j) \in \mathbf{G}_k^{C_j}$  and  $(\mathbf{x}_k, \mathbf{x}_l) \in \mathbf{G}_k^{C_j}$ , and the mutual reachability between  $\mathbf{x}_i$  and  $\mathbf{x}_l$  is the largest of the four points. However, the position of the cluster’s centroid  $\bar{\mathbf{x}}_{C_j}$  influences how well the function represents the centrality in the cluster’s metric space  $(C_j, d_{mreach})$ . We aim to show the current approach strikes a good balance between computational cost and stability in the experiments presented in the next section.



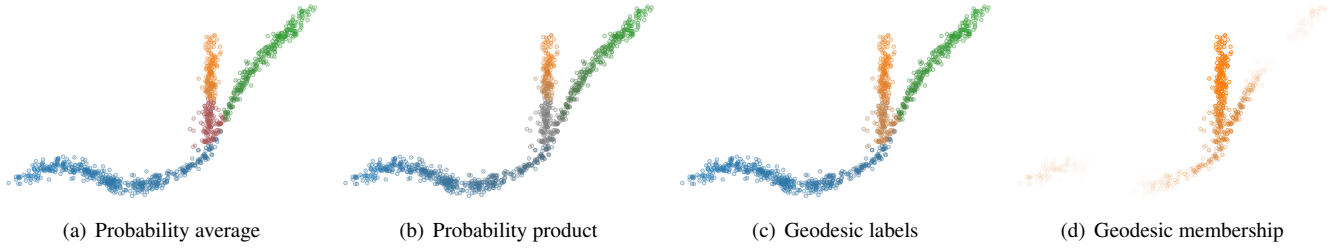


**Figure 3.** Different ways to combine cluster and branch membership probabilities. The cluster and branch probability average (a) and product (b) are visualised with desaturation. (c) Points labelled by the geodesically closest branch root—i.e., the point closest to the branch’s weighted average—and desaturated as in (a). (d) Weighted branch membership for the orange branch is visualised by transparency. Branch memberships are computed from the traversal distance to the branch’s root.

### Computational Complexity

The algorithm’s most computationally expensive steps are constructing the *full cluster approximation graphs* and computing their single linkage hierarchies. Naively, the worst-case complexity for creating a *cluster approximation graph* is  $\mathcal{O}(n_c^2)$ , where  $n_c$  is the number of points in the cluster. Usually, the average case is much better because the approximation graphs rarely are fully connected. After all, HDBSCAN\*’s noise classification limits the density range within the clusters. Furthermore, the *space tree* that we re-use from the HDBSCAN\* clustering step provides fast asymptotic performance for finding the graph’s edges. The exact run-time bounds depend on the data properties. They are challenging to describe (as explained in McInnes and Healy (2017)), but an average complexity proportional to  $\mathcal{O}(n_e \log N)$  is expected, where  $n_e$  is the number of edges in the approximation graph. Computing single linkage hierarchies from the *cluster centrality graphs* is possible in  $\mathcal{O}(n_e \alpha(n_e))$  using McInnes et al. (2017)’s Union-Find implementation adapted to ignore edges between data points that are already in the same connected component ( $\alpha$  is the inverse Ackermann function). Like McInnes and Healy (2017), we feel confident that FLASC achieves sub-quadratic complexity on average, which we demonstrate in a practical example in the next section.

## EXPERIMENTS

Stability and computational performance are essential properties for clustering algorithms to be useful in practice. This section presents two synthetic benchmarks that compare these properties between FLASC’s, HDBSCAN\*, and kMeans. In addition, we demonstrate two exploration use cases where detecting branch-based subgroups and branch hierarchies helps to understand the data’s structure.

### FLASC Stability

This first synthetic benchmark compares the ability of FLASC, HDBSCAN\*, and kMeans to detect branch-based subgroups that do not contain a density maximum. The benchmark is designed to answer the following research question:

How does FLASC’s branch detection ability compare to kMeans and HDBSCAN\* in terms of accuracy and stability?

kMeans was selected for this comparison because it is a popular, fast clustering algorithm that should be able to detect branch-based subgroups when given the correct number of subgroups a priori. HDBSCAN\* was included to show that it cannot reliably find subgroups that do not contain a density maximum, demonstrating that our branch-detection post-processing step enables the algorithm to find an additional type of pattern.

We expect both kMeans and FLASC to be able to detect branching structures, while HDBSCAN\* will struggle due to the lack of density maxima in the to-be-detected subgroups. Furthermore, we expect FLASC to have a higher stability than kMeans—in terms of difference between predictions on multiple samples of the same underlying distribution—as it does not rely on converging from a random initialisation. The next two subsections explain how the data for this benchmark was generated and how we measured the algorithm’s accuracy and stability, respectively.

### Datasets

Two-dimensional data sets containing a single cluster with 3 branches laid out as a three-pointed star were generated (Fig. 4). The branches span from the centre outwards and are spread out equally across the 2D plane—i.e., the angle between adjacent branches is 120 degrees. Each branch has a length  $b_l$  and contains 100 points exponentially spaced from the inside out. Consequently, the density is highest at the cluster’s centre and lowest in the branch ends, and this difference increases with the branch length. Normally distributed noise ( $\mu = 0$ ) is added to the points’ coordinates using a noise ratio parameter  $n_r$  to determine the distribution’s standard deviation  $\sigma$ :

$$n_r = \frac{4\sigma}{\sqrt{\frac{1}{2}b_l}}. \quad (5)$$

Here,  $n_r$  indicates that approximately 95% of the sampled noise values fall within  $\pm\sqrt{\frac{1}{2}n_r b_l}$  of zero. Consequently, approximately 90% of points are moved less than  $n_r b_l$  from their original 2D position.

### Evaluation and settings

The data sets were sampled with varying branch lengths  $b_l$  (2 to 100 in 10 exponentially spaced steps) and noise ratios  $n_r$  (0 to 1 in 10 exponentially spaced steps). Ten data sets were sampled

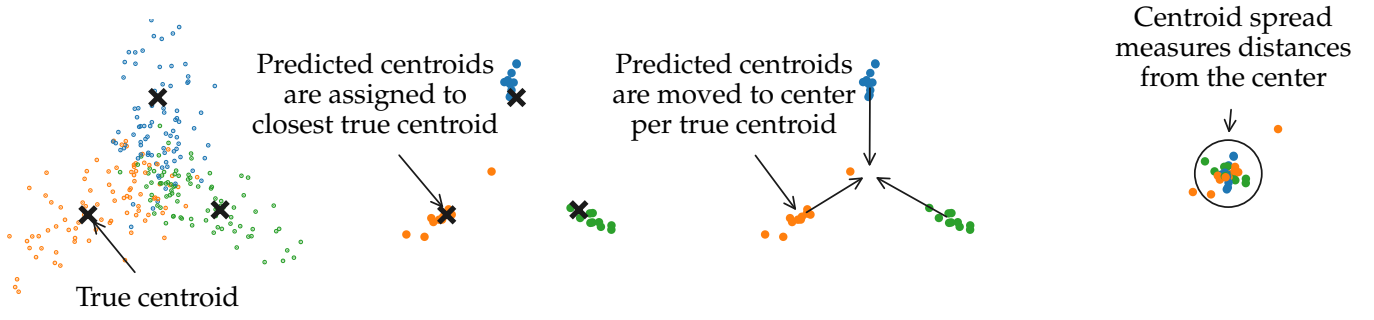


**Figure 4.** Explanatory figure for the centroid spread stability measure. Predicted centroids—weighted average coordinates—are computed for each predicted subgroup and assigned to the closest ground-truth centroid. The 95 percentile centroid spread can be interpreted by translating each group’s average to the origin and finding the radius for a circle that includes 95% of the predicted centroids.

for each parameter combination, resulting in 1000 point clouds. FLASC was tuned to find a single cluster by enabling the *allow single cluster* parameter and setting *min samples*  $k = 5$  and *min cluster size*  $m_c = 25$ . Its branch detection parameters were optimised in a grid search: using the *full* and *core* approximation graphs, both branch selection strategies, and varying the *min branch size*  $m_b$  between 2 to 24 in steps of 2. Labels for central points were set to the geodesically closest branch root (as in Fig. 3(c)). HDBSCAN\* was tuned to find multiple clusters using *min samples*  $k = 5$ . Its other parameters were optimised in a grid search: varying *min cluster size*  $m_c =$  between 2 to 24 in steps of 2, and using both cluster selection strategies. For kMeans, we set  $k = 3$ , using our prior knowledge that there are three branch-based subgroups in the data.

For each evaluation, the resulting data point labels and probabilities were stored and used to compute the Adjusted Rand Index (ARI) (Hubert and Arabie, 1985). ARI values describe the agreement between ground truth and assigned labels adjusted for chance. In addition, the algorithm’s stability was measured using the spread of the predicted branch centroids (see, Fig. 4). Here, the weighted average coordinates per detected subgroup were used as *predicted centroid*. These predicted centroids were assigned to the closest ground-truth centroid. Their spread was quantified as the distance between the predicted centroids and their unweighted average per ground-truth centroid. This value was normalised by the branch length  $b_l$  to allow comparisons across branch lengths.

Finally, we selected the parameter values that maximised the average ARI and minimised the average centroid spread over all data sets. For FLASC, these parameter values were: *min branch size*  $m_b = 12$ , the core cluster approximation graph, and leaf branch selection strategy. Larger values for  $m_b$  provided similar performance values, indicating the algorithm is not very sensitive to  $m_b$  as long as its value is large enough to exclude small noisy structures. HDBSCAN\* performed best with *min cluster size*  $m_c = 8$  and the leaf cluster selection strategy.

## Results

Figure 5(a) demonstrates which subgroups the algorithms detect on a point cloud with  $b_l = 18$  and  $n_r = 0.47$ . The true labels indicate that most confusion is expected in the dense centres,

as the true labels are not spatially separable in those locations. Furthermore, FLASC neatly separated central points by the closest branch. kMeans, on the other hand, generally assigned all central points to one branch and limits the other branches to non-central points. Finally, as expected, HDBSCAN\* did not detect the branch-based subgroups.

The patterns identified in the previous paragraph generalised to other branch lengths and noise ratios, as shown by the average ARI in Fig. 5(b). FLASC achieved ARI values  $\geq 0.8$  on all branch lengths for low noise ratios. Its performance degrades as more noise is introduced, where the decrease in ARI is stronger for large branch lengths. This pattern can be explained by the confusion on central points, as there are more central points with longer branch lengths and larger noise ratios. kMeans achieved ARI values  $\leq 0.8$ . Its performance decreased most strongly with the branch length, which can be explained by the assignment of all central points to one branch.

The 95 percentile centroid spread, shown in Fig. 5(c), indicates FLASC provided more stable results than kMeans. Both algorithms behaved in a similar pattern: the spread was lowest with low noise values and small branch lengths. When either parameter increased, the spread increased as well. However, FLASC achieved lower spread values in these cases, mostly remaining below  $0.25b_l$ . For kMeans, the spread was larger than  $0.25b_l$  in the upper  $b_l - n_r$  triangle. The behaviour on central points explains these patterns.

All in all, this benchmark showed that both FLASC and kMeans are able to detect the branch based subgroups. However, FLASC more accurately segmented the central points, which resulted in a higher accuracy and stability. In addition, FLASC achieved this result without being given the correct number of subgroups a priori.

## Computational Performance

Now we turn to the computational performance. This second synthetic benchmark is designed to answer the following research question:

How does FLASC’s compute cost compare to HDBSCAN\*, kMeans, and fastcluster?

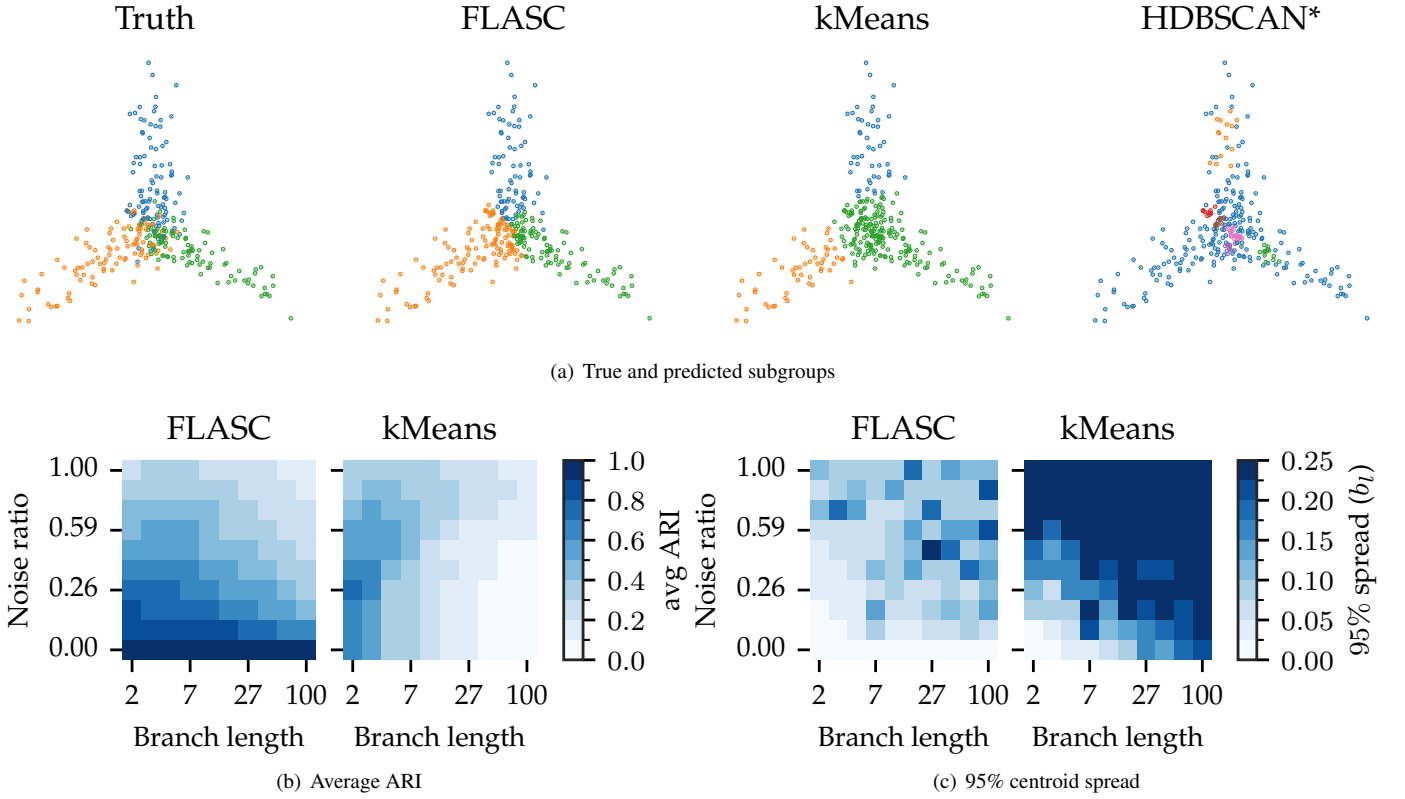


**Figure 5.** Results for the stability benchmark. (a) One point cloud with  $b_l = 18$  and  $n_r = 0.47$  coloured by ground truth and predicted labels that characterise the algorithms’ behaviours. (b) Heatmap with average ARI values for FLASC and kMeans over all branch lengths and noise ratios. (c) Heatmap with 95% centroid spread values for FLASC and kMeans over all branch lengths and noise ratios.

kMeans is included in this comparison because it is a fast, popular clustering algorithm. HDBSCAN\* is included to determine how much extra cost FLASC introduces. Fastcluster is included as an example of a quadratically scaling implementation (as shown in McInnes and Healy (2017)).

Given the challenges in accurately benchmarking the computational performance of algorithms (Kriegel et al., 2017), we limit this comparison to the trends in run time scaling over data set size and number of dimensions for specific implementations.

### Datasets

A Gaussian random walk process was used to generate data sets that contain non-trivially varying densities and branching structures in a controlled environment. For a space with  $d$  dimensions,  $c$  uniform random starting points were sampled in a volume that fits five times the number of to-be-generated clusters. Then, five 50-step random walks were sampled from each starting point. Every step moved along one of the dimensions with a length sampled from a normal distribution ( $\mu = 0$ ,  $\sigma = 0.1$ ). The resulting point clouds have more varied properties than the Gaussian blobs used in McInnes and Healy (2017)’s run time comparison of HDBSCAN\*. Note that the number of (density-based) clusters in each point cloud may differ from the number of starting points  $c$  due to possible overlaps or sparse regions in the random walks.

### Evaluation and settings

The random walk data sets were generated with varying numbers of dimensions (2, 8, 16) and starting points (2 to 800 in 10 exponentially spaced steps). Ten data sets were sampled for each combination of parameters, resulting in a total of 300 point clouds.

The algorithms were compared using their Python implementations: fastcluster version 1.1.26 (Müllner, 2013), kMeans version 1.3.2 (Pedregosa et al., 2011), HDBSCAN\* version 0.8.28 (McInnes et al., 2017), and FLASC version 0.1.3 with the *full* and *core* approximation graphs. HDBSCAN\* and FLASC were evaluated with *min samples*  $k = 10$ , *min cluster size*  $m_c = 100$ , *min branch size*  $m_b = 20$ , *allow single cluster* enabled, and their multiprocessing support disabled to better describe the algorithms’ intrinsic complexity. These parameter values allow the algorithms to find clusters and branches that are slightly smaller than how they are generated. Fastcluster’s default parameter values were used, resulting in a single linkage dendrogram. kMeans was evaluated with  $k = c$ , effectively attempting to recover one cluster for each starting point.

Time measurements were performed with a 5.4GHz AMD R7 7700X processor. Each algorithm was evaluated on each data set once, recording the run time and number of detected clusters. The smallest data set for which an algorithm required more than 80 seconds was recorded for each number of dimensions. Larger data sets were not evaluated for those algorithms.



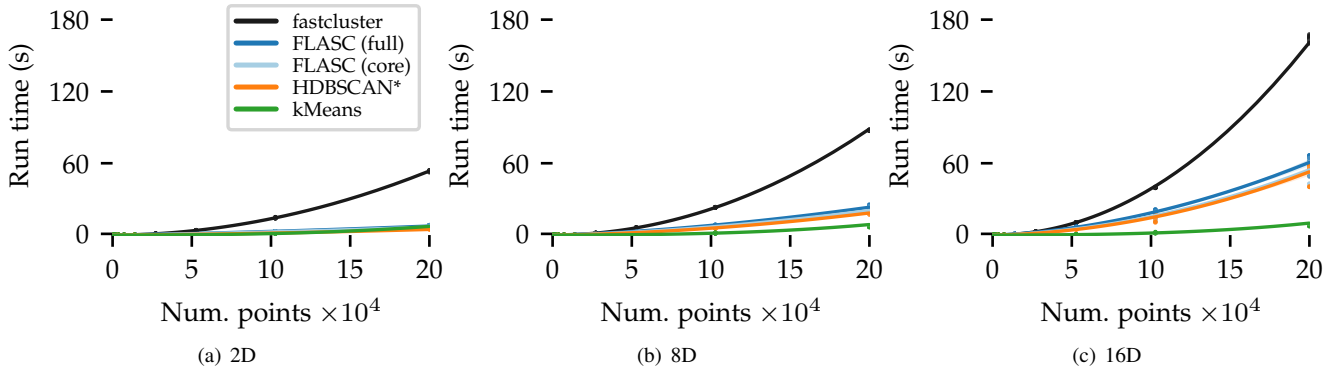


**Figure 6.** Benchmark run times (s) over the data set size and number of dimensions. The algorithms’ scaling behaviours are visualised by quadratic regression lines relating compute time to the number of points in log–log space, shown in linear space. The shaded areas around each line indicate the regression’s 95% confidence interval.

## Results

Figure 6 shows run times in seconds over the data set size and number of dimensions. There are three patterns of note. Firstly, *fastcluster* shows the steepest quadratic trend, resulting in the longest run times. *FLASC* and *HDBSCAN\** show shallower trends on the 2 and 8 dimensional data sets but approach *fastcluster*’s quadratic trend in the 16 dimensional case. This is expected because querying *space trees* becomes more expensive with more dimensions (Weber et al., 1998). Secondly, *HDBSCAN\** and both *FLASC* variants scale similarly in all three conditions. *HDBSCAN\** is consistently the fastest of the three, followed by *FLASC* with the *core* approximation graph. However, their run time differences diminish in the higher dimensional cases, indicating that the additional cost of branch detection is relatively low compared to the cost of detecting the clusters. Finally, *kMeans* had the shallowest scaling trend in all three conditions, indicating that it is the fastest algorithm of the four.

In conclusion, both *FLASC* variants’ computational performance scale similarly to *HDBSCAN\** and the more dimensions the data contains, the smaller the scaling trend differences between the algorithms.

## Use Case: Diabetes Types

Next, we present a data exploration case in which identifying branch-based subgroups is essential to understand the data. Reaven and Miller (1979) attempted to clarify a “horse shoe”-shaped relation between glucose levels and insulin responses in diabetes patients. Three of the metabolic variables they measured turned out to be very informative in a 3D scatterplot, showing a dense core with two less-dense branches, which they considered unlikely to be a single population. Seeing that plot was instrumental in their understanding of the data (Miller, 1985).

More recently, Singh et al. (2007) used the same data set to demonstrate how Mapper with a density-based lens function visualises these flares without manually specifying which dimensions to plot. Their analysis leverages the flares’ lower density, allowing them to be detected without a centrality metric.

In general, though, local density minima do not always relate to branches, especially for data sets with multiple branching clusters.

In this use case, we show how *FLASC* can detect the branching pattern in this data set and classify the observations by their branch without manually extracting the flares from a visualisation.

## Evaluation and settings

The data set—obtained from Andrews and Herzberg (1985)—contains five variables describing 145 subjects: the relative weight, the plasma glucose level after a period of fasting, the steady-state plasma glucose response (SSPG), and two areas under a curve—one for glucose (AUGC) and one for insulin (AUCI)—representing the total amount observed during the experimental procedure described in Reaven and Miller (1979). All five variables were z-score normalised and used to compute the Euclidean distance between subjects.

Both *FLASC* and *HDBSCAN\** were evaluated on the normalised data set. *FLASC* was tuned to find a single cluster with multiple branches by setting *min samples*  $k = 5$ , *min cluster size*  $m_c = 100$ , *min branch size*  $m_b = 5$ , and enabling *allow single cluster*. *HDBSCAN\** was tuned to find multiple clusters with *min samples*  $k = 5$  and *min cluster size*  $m_c = 10$ .

## Results

Figure 7 shows the detected subgroups encoded using colour on the 3D scatterplot. *FLASC*’s classification (Fig. 7(a)) distinguishes the branches from the central core. The algorithm also finds a low-persistent flare representing the central core’s bottom. This flare could be ignored by specifying a persistence threshold. In contrast, *HDBSCAN\**’s classification (Fig. 7(b)) does not find the branches. Instead, it finds part of the left branch as a small low-persistent cluster and merges most of the right branch with the central core.

All in all, this case study demonstrated how *FLASC* detects branch-based subgroups that do not contain local density maxima without having to specify the relevant features in advance or extract the subgroups visually. Practically, *FLASC* would have made it easier for researchers to detect the three groups in

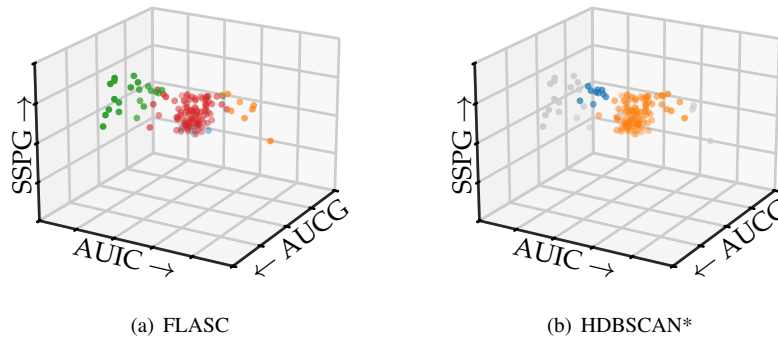


**Figure 7.** Subgroups detected by (a) FLASC and (b) HDBSCAN\* shown in a 3D scatterplot over the area under the plasma glucose curve (AUGC), the area under the insulin curve (AUIC), and the steady state plasma glucose response (SSPG) from Reaven and Miller (1979). Grey points were classified as noise.

this data set, which was relevant for understanding diabetes and its causes.

### Use Case: Cell Development

Finally, we demonstrate a use case where detecting a branch hierarchy is important for understanding the data set. Specifically, we analyse Packer et al. (2019)’s cell development atlas for the *C. Elegans*, a small roundworm that is often used in biological studies. They analysed gene expressions in *C. Elegans* embryos to uncover the trajectories along which cells develop. Broadly speaking, this data set describes what happens in cells as they develop from a single egg cell into all the different tissues that exist within fully grown *C. Elegans* worms.

After pre-processing, the data set appears to contain both cluster and branching structures when viewed in Packer et al. (2019)’s 3D projection. In this use case, we demonstrate that FLASC’s branch hierarchy provides interesting information about the data set’s structure even when the main subgroups can be detected as clusters.

### Evaluation and settings

The data and pre-processing scripts were obtained from Monocle 3’s (Cao et al., 2019) documentation (Pliner et al., 2022). The pre-processing stages normalise the data, extract the 50 strongest PCA components, and correct for batch effects using algorithms from Haghverdi et al. (2018). HDBSCAN\* was evaluated on the pre-processed data with an angular distance metric because the cosine distance metric is not supported in its optimised code path. HDBSCAN\* was tuned to find multiple clusters with *min samples*  $k = 5$  and *min cluster size*  $m_c = 50$ . FLASC was evaluated on a 3D UMAP (McInnes et al., 2020) projection that denoised the data set. Using three instead of two dimensions reduces the chance of branch overlaps in the embedding. UMAP used the angular distance metric to find 30 nearest neighbours. The *disconnection distance* parameter was set to exclude the 16-percentile least dense points detected by HDBSCAN\*, thereby preventing shortcuts across the data’s structure. The largest connected component in the resulting UMAP graph was projected to 3D while varying the repulsion strength to avoid crossings and ensure connected structures re-

mained close. The same layout procedure was used to project the graph to 2D to visualise the data. FLASC was tuned to detect the branching hierarchy of the dataset as a single cluster by selecting *min samples*  $k = 3$ , *min cluster size*  $m_c = 500$ , *min branch size*  $m_b = 50$ , enabling *allow single cluster*. Branches were detected using the *core* cluster approximation graph and selected with the leaf strategy.

### Results

Figures 8(b) and 8(a) show the 2D projections. Data points are coloured to indicate the detected clusters and branches, respectively. There are two main differences between the branches and the clusters. Firstly, two regions where branches merge are detected as clusters, namely clusters 10 and 14. These regions do not have a distinct branch label, but are identifiable in the branch hierarchy (Fig. 8(d)). Secondly, all but one branch—branch 13—are also detected as a cluster in this dataset, indicating the branches represent regions with high local density. Considering that the branches correspond to developmental end-states, it is unsurprising that local density maxima occur within them. One could imagine that the variation in gene expression is higher during development and that fully developed cells are observed more frequently. Both scenarios could cause these local density maxima.

More interesting are the differences between the cluster and branch hierarchies. Figures 8(c) and 8(d) visualise these hierarchies as an icicle plot. These designs are adapted from McInnes et al. (2017) to indicate the selected branches and clusters using colour and a label. Segment widths encode the number of points in the tree below the segment. The hierarchies highlight that while HDBSCAN\* detects the branches as clusters, it does not capture the trajectories. For example, the hierarchy does not reflect that clusters 0 and 1 connect to the whole data set through cluster 10. FLASC’s branch hierarchy, on the other hand, more closely resembles the data’s shape. For example, the hierarchy describes the embedding’s left and right side with 5 and 6 branches, respectively. In general, branches that merge into the cluster near each other are also close in the branch condensed tree. For branches connected to multiple other branches in the cluster approximation graph, only the most eccentric connection

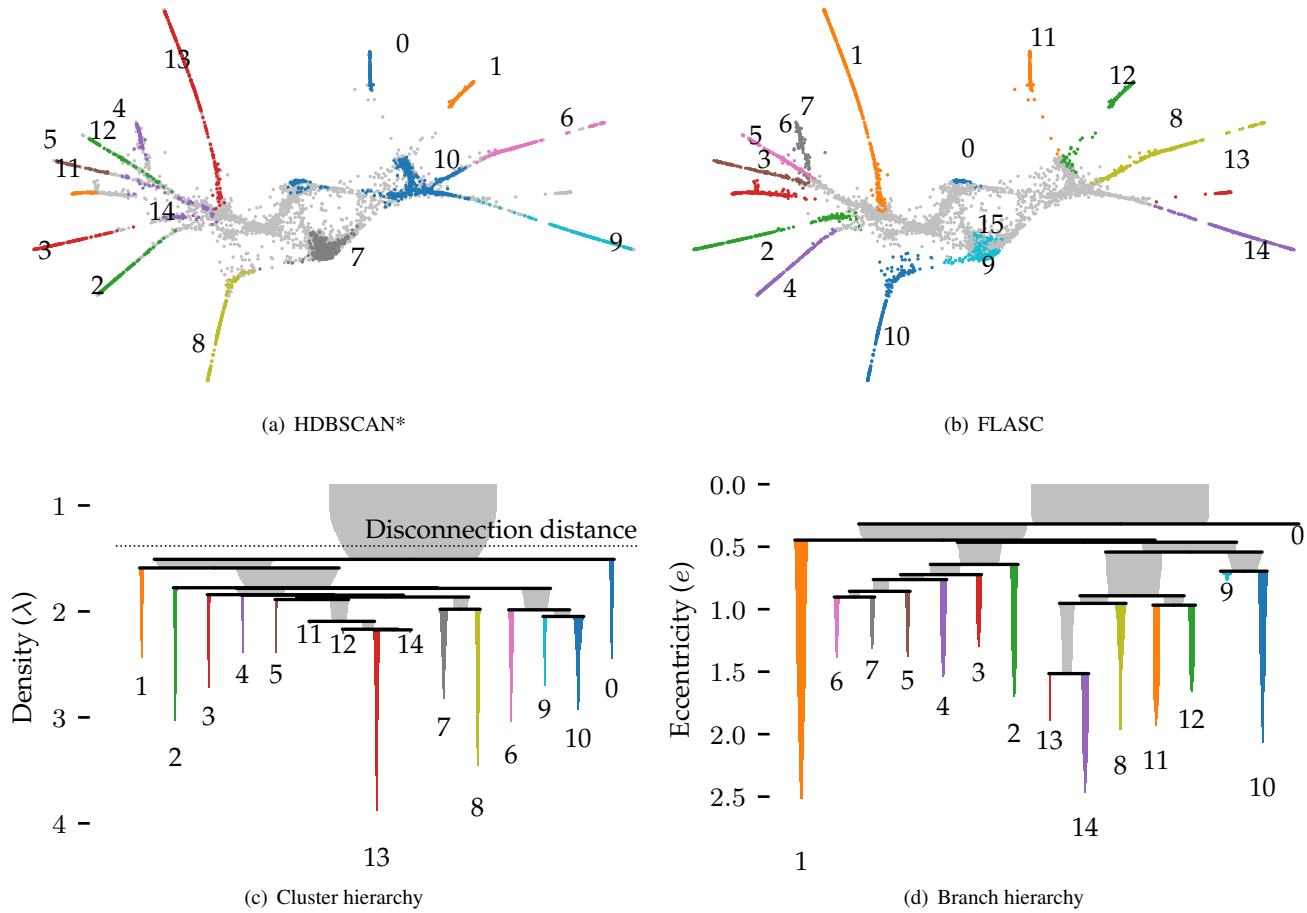


**Figure 8.** Results for the single cell gene expression use case using 50 dimensional pre-processed data from Packer et al. (2019). (a) 2D UMAP projection (McInnes et al., 2020) coloured by HDBSCAN\* clusters detected in the pre-processed data. (b) The same projection coloured by FLASC branches detected from a 3D UMAP projection. (c) and (d) show cluster and branch hierarchies, respectively. The icicle plots were adapted from McInnes et al. (2017) to indicate selected clusters with colour and labels.

is captured by the branch-condensed tree.

All in all, this use case demonstrated that FLASC’s branch hierarchy provides information about the data’s shape that may not be obvious from cluster hierarchies. In addition, we found it beneficial to suppress noisy connectivity using dimensionality reduction techniques when detecting branches.

## DISCUSSION

Two synthetic benchmarks and two real-world use cases were performed to demonstrate FLASC and its properties. We start our discussion by providing remarks for each benchmark and use case in order.

The stability benchmark compared FLASC and kMeans in their ability to detect branches that do not contain a density maximum. The benchmark quantified performance in terms of ARI and a centroid spread measure that describes output similarity between multiple samples of the same underlying distribution. While both algorithms were able to detect the branches, FLASC performed better than kMeans on both measures. In addition, kMeans requires specifying the correct number of subgroups a priori, which is difficult with unfamiliar data. This analysis

could be expanded to investigate how well FLASC deals with unequal branch lengths. The weighted average data point—and eccentricity measure as a result—may not accurately reflect the centre of such clusters. Consequently, FLASC’s branch hierarchy will be a less accurate representation of the underlying topology but should still detect the branches. Monocle 3 (Qiu et al., 2017) deals with this problem by selecting the centre point in a projection manually (Pliner et al., 2022). Other eccentricity measures discussed below could also improve FLASC’s performance in such cases.

The computational performance benchmark demonstrated that FLASC’s computational performance scales similar to HDBSCAN\*. The scaling trends appear to become more similar as the data contained more dimensions. Neither algorithm was evaluated with multiprocessing enabled, which can introduce run-time differences in practical applications. In addition, extracting the *full* cluster approximation graph can be more expensive than reported, depending on the data’s characteristics. kMeans provided even quicker run times, but is limited in usability due to lower stability and its predefined number of clusters.

The diabetes types use case demonstrated a real-world

dataset in which branches that are not detectable as density-based clusters represent meaningful subgroups. FLASC is designed to detect such branches without knowing they exist a priori or extracting them from a visualisation manually. The cell development use case showed how FLASC behaves on a more complex data set. Here, the subgroups were detectable by both FLASC and HDBSCAN\*. FLASC still provides a benefit for exploration because its branch hierarchy more closely resembles the data's shape. Structure learning algorithms, as described in Section "Related Work – Structure Learning", can provide even more information about the data's shape at more computational costs.

### FLASC's practical value

As demonstrated by the cell development use case, the argument that branches are not detectable as clusters only applies when they do not contain local density maxima. Subpopulations tend to have some location in feature space where observations are more likely. These locations are detectable as local density maxima, allowing data points surrounding them to be classified as a particular cluster. If one is only interested in the existence of subgroups, then FLASC only provides a benefit on datasets where relevant subgroups are sparse (e.g., the diabetes types use case). If one is also interested in the clusters' shapes, then FLASC's branch hierarchy provides information that cannot be extracted from a cluster hierarchy. We envision FLASC as a valuable tool for exploring unfamiliar data, providing guidance into which subpopulations exist and informing follow-up questions. Knowing that a cluster may represent multiple subgroups can be very relevant.

### Alternative eccentricity metrics

The presented FLASC algorithm uses a geometric distance-to-centroid metric to describe how eccentric data points are within a cluster (Fig. 2(a), Eq. 3). An interesting alternative is an unweighted geodesic eccentricity, which measures path-lengths between each data point and the cluster's root point in the cluster approximation graph. Here, the root point can be chosen as the data point closest to the cluster's centroid, as we did for the branch-membership vectors (Fig. 3). Such a geodesic eccentricity would agree with the notion that distances in high dimensional data may not accurately reflect distances along the intrinsic structure of a data set, which was one of the motivations for Reversed Graph Embeddings (Mao et al., 2017). It would also be closer to the maximum shortest-path centrality metric used by (Vandaele et al., 2021).

Several trade-offs between the geometric and geodesic eccentricity metrics made us choose the geometric one:

- Computing the geodesic eccentricity is more expensive because it requires an additional traversal over the entire cluster approximation graph. The extra cost, however, should be low compared to other parts of the algorithm.
- The resolution of the unweighted geodesic eccentricity is lower, as it expresses the number of edges to the root point. As a result, zero-persistent branches are more likely to occur. In addition, it reduces the detectability of small branches that are well connected. On the other hand, that

can be seen as beneficial noise suppression. In addition, the *branch selection persistence* parameter becomes more interpretable and would represent the traversal depth of a branch in the approximation graph.

- The cluster's centroid may lie outside of the cluster itself, resulting in a root point and eccentricity values that do not accurately describe its centre. For example, imagine a U-shaped cluster. The centroid would lie in between the two arms, and the root would lie in one of the arms. As a result, the geodesic metric would find one smaller and one larger branch rather than two equal branches. On the other hand, the geometric eccentricity finds the two branches and the connecting bend as three separate groups. Confusingly, it also contains two regions with a local eccentricity maximum, which FLASC gives a single label. Placing the root at an arbitrary eccentric location as in Ge et al. (2011) avoids this issue but necessitates a different interpretation of the branch hierarchy and branch probability.

FLASC's general process can also be used with metrics that capture other aspects than eccentricity. At its core, FLASC consists of two filtrations, one to determine the connectivity between data points and one to analyse a signal on the resulting graph. The process would then describe how many distinct local minima (or maxima) of the metric exist within the clusters. The resulting interpretation does not have to relate to the cluster's shape.

One could even interpret FLASC as two applications of HDBSCAN\*: one over the density and one over the eccentricity. This perspective raises a possible improvement to the algorithm by translating the mutual reachability concept to the centrality metric. The idea of 'pushing away points in low-density regions' can also be applied to the centrality and would emphasise the centrality difference between the centre and branch ends. Additionally, smoothing the centrality profile by incorporating neighbouring values could improve the algorithm's robustness to noise. The additional computational cost should be low, as points' neighbours are already known when the centrality is computed. Another way to improve noise robustness could be to implement the *mutual k*-nearest neighbour approach used by Dalmia and Sia (2021) to improve UMAP projections. It would provide a subgraph of the *core* approximation graph that better reflects the cluster's connectivity in high dimensional data sets. We leave evaluating these ideas for future work.

### Visually summarising data's shape

A strength of Mapper (Singh et al., 2007) and Reversed Graph Embeddings (Mao et al., 2017) is that they can summarise the data's shape using intuitive visualisations. While FLASC's branch-condensed tree provides some information about the clusters' shapes, interpreting the shape is not trivial. Studying how well two-dimensional layouts of FLASC's cluster approximation graphs work as shape summarising visualisations would be an interesting future research direction. These graphs directly encode the connectivity used by the algorithm. Another benefit is that—unlike in Mapper—all (non-noise) data points are represented in the graphs once. Directly visualising the



graphs, however, probably does not scale to larger sizes in terms of computational cost for the layout algorithm and visual interpretability. Ways to summarise the networks would have to be found, which could be based on kMeans centroids like in Reversed Graph Embeddings (Mao et al., 2017), local density maxima in the cluster, or a Reeb-Graph approach similar to Ge et al. (2011).

## CONCLUSION

We presented the FLASC algorithm that combines HDBSCAN\* clustering with branch-detection post-processing step. We have shown that the algorithm can detect branch-based subgroups that do not contain local density maxima in real-world data without specifying features of interest or extracting the branches from a visualisation manually. In addition, we demonstrated that branching hierarchies found by FLASC can provide information about the data's shape that is not present in HDBSCAN\*'s cluster hierarchy. Two synthetic benchmarks demonstrated FLASC's stability and indicated FLASC's computational performance scales similarly to HDBSCAN\*.

## ACKNOWLEDGEMENTS

We thank Kris Luyten for his comments on an early version of the manuscript.

## DATA AVAILABILITY

The data and code used in this paper are available at <https://zenodo.org/records/13326252>.

## FUNDING STATEMENT

The work of D.M. Bot was supported by Hasselt University BOF grant [BOF20OWB33]. The work of J. Peeters was supported by Hasselt University BOF grant [BOF21DOC19]. The work of J. Aerts was supported by KU Leuven grant STG/23/040.

## REFERENCES

Andrews, D. F. and Herzberg, A. M. Chemical and Overt Diabetes. In *Data A Collect. Probl. from Many Fields Student Res. Work.*, pages 215–220. Springer New York, New York, NY, 1985. doi:10.1007/978-1-4612-5098-2\_37.

Belkin, M. and Niyogi, P. Laplacian eigenmaps for dimensionality reduction and data representation. *Neural Comput.*, 15(6):1373–1396, 2003. doi:10.1162/089976603321780317.

Bonnaire, T., Decelle, A., and Aghanim, N. Regularization of Mixture Models for Robust Principal Graph Learning. *IEEE Trans. Pattern Anal. Mach. Intell.*, 44(12):9119–9130, 2022. doi:10.1109/tpami.2021.3124973.

Botnan, M. B., Oppermann, S., Oudot, S., and Scoccola, L. On the bottleneck stability of rank decompositions of multi-parameter persistence modules. arXiv:2208.00300 [math.AT], 2022.

Campello, R. J., Moulavi, D., and Sander, J. Density-Based Clustering Based on Hierarchical Density Estimates. In *Pacific-Asia conference on knowledge discovery and data*

*mining*, pages 160–172, Berlin, Heidelberg, Germany, 2013. Springer. doi:10.1007/978-3-642-37456-2\_14.

Campello, R. J. G. B., Moulavi, D., Zimek, A., and Sander, J. Hierarchical Density Estimates for Data Clustering, Visualization, and Outlier Detection. *ACM Trans. Knowl. Discov. Data*, 10(1):1–51, July 2015. doi:10.1145/2733381.

Cao, J., Spielmann, M., Qiu, X., Huang, X., Ibrahim, D. M., Hill, A. J., Zhang, F., Mundlos, S., Christiansen, L., Steemers, F. J., Trapnell, C., and Shendure, J. The single-cell transcriptional landscape of mammalian organogenesis. *Nature*, 566(7745):496–502, Feb. 2019. doi:10.1038/s41586-019-0969-x.

Carlsson, G. Topological pattern recognition for point cloud data. *Acta Numer.*, 23(2014):289–368, May 2014. doi:10.1017/s0962492914000051.

Chazal, F., Cohen-Steiner, D., Guibas, L. J., Méholi, F., and Oudot, S. Y. Gromov-Hausdorff Stable Signatures for Shapes using Persistence. *Comput. Graph. Forum*, 28(5):1393–1403, July 2009. doi:10.1111/j.1467-8659.2009.01516.x.

Chervov, A., Bac, J., and Zinovyev, A. Minimum Spanning vs. Principal Trees for Structured Approximations of Multi-Dimensional Datasets. *Entropy*, 22(11):1274, Nov. 2020. doi:10.3390/e22111274.

Dalmia, A. and Sia, S. Clustering with UMAP: Why and How Connectivity Matters. arXiv:2108.05525 [cs.AI], 2021.

Dempster, A. P., Laird, N. M., and Rubin, D. B. Maximum Likelihood from Incomplete Data Via the EM Algorithm. *J. R. Stat. Soc. Ser. B Stat. Methodol.*, 39(1):1–22, Sept. 1977. doi:10.1111/j.2517-6161.1977.tb01600.x.

Dong, W., Moses, C., and Li, K. Efficient k-nearest neighbor graph construction for generic similarity measures. In *Proc. 20th Int. Conf. World wide web*, pages 577–586, New York, NY, USA, Mar. 2011. Acm. ISBN 9781450306324. doi:10.1145/1963405.1963487.

Doraiswamy, H., Tierny, J., Silva, P. J. S., Nonato, L. G., and Silva, C. Topomap: A 0-dimensional homology preserving projection of high-dimensional data. *IEEE Transactions on Visualization and Computer Graphics*, 27(2):561–571, 2021. doi:10.1109/tvcg.2020.3030441.

Ester, M., Kriegel, H.-P., Sander, J., and Xu, X. A Density-Based Algorithm for Discovering Clusters in Large Spatial Databases with Noise. In *Proc. 2nd Int. Conf. Knowl. Discov. Data Min.*, pages 226–231, Portland, OR, USA, 1996. AAAI Press.

Ge, X., Wang, Y., Safa, I., Belkin, M., and Wang, Y. Data Skeletonization via Reeb Graphs. In Shawe-Taylor, J., Zemel, R., Bartlett, P., Pereira, F., and Weinberger, K. Q., editors, *Adv. Neural Inf. Process. Syst.*, volume 24, pages 1–9. Curran Associates, Inc., 2011.

Haghverdi, L., Lun, A. T. L., Morgan, M. D., and Marioni, J. C. Batch effects in single-cell RNA-sequencing data are corrected by matching mutual nearest neighbors. *Nat. Biotechnol.*, 36(5):421–427, May 2018. doi:10.1038/nbt.4091.

Hartigan, J. A. *Clustering algorithms*, volume 209. Wiley, New York, NY, USA, 1975.

Hastie, T. and Stuetzle, W. Principal Curves. *J. Am. Stat. Assoc.*, 84(406):502–516, June 1989. doi:10.1080/01621459.1989.10478797.

- Hubert, L. and Arabie, P. Comparing partitions. *J. Classif.*, 2(1):193–218, Dec. 1985. doi:10.1007/bf01908075.
- Jackson, J., Qiao, A., and Xing, E. P. Scaling HDBSCAN Clustering with KNN Graph Approximation. In *Proceedings of the SysML Conference*, pages 14–16, Stanford, CA, USA, 2018.
- Kamruzzaman, M., Kalyanaraman, A., and Krishnamoorthy, B. Detecting Divergent Subpopulations in Phenomics Data using Interesting Flares. In *Proc. 2018 ACM Int. Conf. Bioinformatics, Comput. Biol. Heal. Informatics*, pages 155–164, New York, NY, USA, Aug. 2018. Acm. ISBN 9781450357944. doi:10.1145/3233547.3233593.
- Kerber, M. and Rolle, A. Fast Minimal Presentations of Bigraded Persistence Modules. In *2021 Proc. Work. Algorithm Eng. Exp.*, pages 207–220. Society for Industrial and Applied Mathematics, Philadelphia, PA, USA, Jan. 2021. ISBN 9781611976472. doi:10.1137/1.9781611976472.16.
- Kriegel, H.-P., Schubert, E., and Zimek, A. The (black) art of runtime evaluation: Are we comparing algorithms or implementations? *Knowledge and Information Systems*, 52(2): 341–378, 2017. doi:10.1007/s10115-016-1004-2.
- Lesnick, M. and Wright, M. Interactive visualization of 2-d persistence modules. arXiv:1512.00180 [math.AT], 2015.
- Lesnick, M. and Wright, M. Computing minimal presentations and bigraded betti numbers of 2-parameter persistent homology. arXiv:1902.05708 [math.AT], 2022.
- Li, M., Duncan, K., Topp, C. N., and Chitwood, D. H. Persistent homology and the branching topologies of plants. *Am. J. Bot.*, 104(3):349–353, 2017. doi:10.3732/ajb.1700046.
- Lum, P. Y., Singh, G., Lehman, A., Ishkanov, T., Vejdemo-Johansson, M., Alagappan, M., Carlsson, J., and Carlsson, G. Extracting insights from the shape of complex data using topology. *Sci. Rep.*, 3(1):1–8, Feb. 2013. doi:10.1038/srep01236.
- Malzer, C. and Baum, M. A Hybrid Approach To Hierarchical Density-based Cluster Selection. In *2020 IEEE Int. Conf. Multisens. Fusion Integr. Intell. Syst.*, volume 2020-Sept, pages 223–228, Karlsruhe, Germany, Sept. 2020. Ieee. ISBN 978-1-7281-6422-9. doi:10.1109/mfi49285.2020.9235263.
- Mao, Q., Wang, L., Tsang, I. W., and Sun, Y. Principal Graph and Structure Learning Based on Reversed Graph Embedding. *IEEE Trans. Pattern Anal. Mach. Intell.*, 39(11):2227–2241, 2017. doi:10.1109/tpami.2016.2635657.
- McInnes, L. and Healy, J. Accelerated hierarchical density based clustering. In *2017 IEEE International Conference on Data Mining Workshops (ICDMW)*, pages 33–42, New Orleans, LA, USA, 2017. Ieee. doi:10.1109/icdmw.2017.12.
- McInnes, L., Healy, J., and Astels, S. hdbscan: Hierarchical density based clustering. *The Journal of Open Source Software*, 2(11):205, 2017. doi:10.21105/joss.00205.
- McInnes, L., Healy, J., and Melville, J. UMAP: Uniform Manifold Approximation and Projection for Dimension Reduction. arXiv:1802.03426 [stat.ML], 2020.
- McInnes, L., Healy, J., and Astels, S. HDBSCAN Documentation: How Soft Clustering for HDBSCAN Works. [https://hdbscan.readthedocs.io/en/latest/soft\\_clustering\\_explanation.html](https://hdbscan.readthedocs.io/en/latest/soft_clustering_explanation.html), 2022. Accessed: 2022-12-09, Revision: 109797c7.
- Miller, R. G. Discussion: Projection Pursuit. *Ann. Stat.*, 13(1): 510–513, 1985.
- Müllner, D. fastcluster: Fast hierarchical, agglomerative clustering routines for r and python. *Journal of Statistical Software*, 53(9):1–18, 2013. doi:10.18637/jss.v053.i09.
- Neto, A. C. A., Nascimento, M. A., Sander, J., and Campello, R. J. G. B. MustACHE. *Proc. VLDB Endow.*, 11(12):2058–2061, Aug. 2018. doi:10.14778/3229863.3236259.
- Neto, A. C. A., Sander, J., Campello, R. J., and Nascimento, M. A. Efficient Computation and Visualization of Multiple Density-Based Clustering Hierarchies. *IEEE Trans. Knowl. Data Eng.*, 33(8):3075–3089, 2021. doi:10.1109/tkde.2019.2962412.
- Packer, J. S., Zhu, Q., Huynh, C., Sivaramakrishnan, P., Preston, E., Dueck, H., Stefanik, D., Tan, K., Trapnell, C., Kim, J., Waterston, R. H., and Murray, J. I. A lineage-resolved molecular atlas of *C. elegans* embryogenesis at single-cell resolution. *Science*, 365(6459):eaax1971, Sept. 2019. doi:10.1126/science.aax1971.
- Pedregosa, F., Varoquaux, G., Gramfort, A., Michel, V., Thirion, B., Grisel, O., Blondel, M., Prettenhofer, P., Weiss, R., Dubourg, V., et al. Scikit-learn: Machine learning in python. *the Journal of machine Learning research*, 12(85):2825–2830, 2011.
- Pliner, H. A., Kouhei, S., and Trapnell, C. Monocle 3 Documentation: Constructing single-cell trajectories. <https://cole-trapnell-lab.github.io/monocle3/docs/trajectories/>, 2022. Accessed: 2023-05-04, Revision: 0d1cf4d.
- Qiu, X., Mao, Q., Tang, Y., Wang, L., Chawla, R., Pliner, H. A., and Trapnell, C. Reversed graph embedding resolves complex single-cell trajectories. *Nat. Methods*, 14(10):979–982, Oct. 2017. doi:10.1038/nmeth.4402.
- Reaven, G. M. and Miller, R. G. An attempt to define the nature of chemical diabetes using a multidimensional analysis. *Diabetologia*, 16(1):17–24, Jan. 1979. doi:10.1007/bf00423145.
- Roweis, S. T. and Saul, L. K. Nonlinear dimensionality reduction by locally linear embedding. *Science*, 290(5500): 2323–2326, 2000. doi:10.1126/science.290.5500.2323.
- Scoccola, L. and Rolle, A. Persistable: persistent and stable clustering. *J. Open Source Softw.*, 8(83):5022, 2023. doi:10.21105/joss.05022.
- Sibson, R. SLINK: An optimally efficient algorithm for the single-link cluster method. *The Computer Journal*, 16(1): 30–34, Jan. 1973. doi:10.1093/comjnl/16.1.30.
- Singh, G., Memoli, F., and Carlsson, G. Topological Methods for the Analysis of High Dimensional Data Sets and 3D Object Recognition. In Botsch, M., Pajarola, R., Chen, B., and Zwicker, M., editors, *Eurographics Symposium on Point-Based Graphics*. The Eurographics Association, 2007. ISBN 978-3-905673-51-7. doi:10.2312/SPBG/SPBG07/091-100.
- Skaf, Y. and Laubenbacher, R. Topological data analysis in biomedicine: A review. *J. Biomed. Inform.*, 130(November 2021):104082, 2022. doi:10.1016/j.jbi.2022.104082.
- Stewart, G. and Al-Khassaweneh, M. An Implementation of the HDBSCAN\* Clustering Algorithm. *Appl. Sci.*, 12(5):2405, Feb. 2022. doi:10.3390/app12052405.
- Tenenbaum, J. B., de Silva, V., and Langford, J. C. A

- global geometric framework for nonlinear dimensionality reduction. *Science*, 290(5500):2319–2323, 2000. doi:10.1126/science.290.5500.2319.
- Toussaint, G. T. The relative neighbourhood graph of a finite planar set. *Pattern Recognit.*, 12(4):261–268, Jan. 1980. doi:10.1016/0031-3203(80)90066-7.
- van der Maaten, L. and Hinton, G. Visualizing data using t-SNE. *J. Mach. Learn. Res.*, 9(86):2579–2625, Nov. 2008.
- Vandaele, R., Saeys, Y., and De Bie, T. Mining topological structure in graphs through forest representations. *J. Mach. Learn. Res.*, 21:1–68, 2020.
- Vandaele, R., Rieck, B., Saeys, Y., and De Bie, T. Stable topological signatures for metric trees through graph approximations. *Pattern Recognit. Lett.*, 147:85–92, July 2021. doi:10.1016/j.patrec.2021.03.035.
- Weber, R., Schek, H.-J., and Blott, S. A quantitative analysis and performance study for similarity-search methods in high-dimensional spaces. In *VLDB*, volume 98, pages 194–205, 1998.
- Wishart, D. Mode analysis, a generalization of nearest neighbour which reduces chaining. In Cole, A. J., editor, *Numerical Taxonomy*, pages 282–311, London, New York, 1969. Academic Press. ISBN 0121796507.